Jokinen, Ville; Suvanto, Pia; Garapaty, Anshul Rao; Lyytinen, Jussi; Koskinen, Jari; Franssila, Sami

Durable superhydrophobicity in embossed CYTOP fluoropolymer micro and nanostructures

Published in:
Colloids and Surfaces A: Physicochemical and Engineering Aspects

DOI:
10.1016/j.colsurfa.2013.05.061

Published: 05/10/2013

Document Version
Peer-reviewed accepted author manuscript, also known as Final accepted manuscript or Post-print

Please cite the original version:
Jokinen, V., Suvanto, P., Garapaty, A. R., Lyytinen, J., Koskinen, J., & Franssila, S. (2013). Durable superhydrophobicity in embossed CYTOP fluoropolymer micro and nanostructures. *Colloids and Surfaces A: Physicochemical and Engineering Aspects*, *434*, 207-212. https://doi.org/10.1016/j.colsurfa.2013.05.061

The final publication is available from the publisher at:
http://dx.doi.org/10.1016/j.colsurfa.2013.05.061

Durable Superhydrophobicity in Embossed CYTOP Fluoropolymer Micro and Nanostructures

Ville Jokinen*, Pia Suvanto, Anshul Rao Garapaty, Jussi Lyytinen, Jari Koskinen and Sami Franssila

Department of Materials Science and Engineering, School of Chemical Technology, Aalto University

Tietotie 3, 02150, Espoo, Finland, *E-mail: ville.p.jokinen@aalto.fi. Tel:+3580504602892

Abstract:

Micropillars, nanopillars and dual scale micro-nanopillars were fabricated out of an inherently hydrophobic amorphous CYTOP fluoropolymer by hot embossing. The resulting pillars were superhydrophobic with high apparent contact angles ($\theta > 160^\circ$) and low rolling angles. Abrasion experiments were performed using a novel rotary abrasive slurry setup. Due to their inherent hydrophobicity, CYTOP micro and nanopillars retained their superhydrophobic properties even after 4 hours of abrasion (900 rpm in 10 % slurry of 30 μm alumina particles), unlike control samples prepared out of fluoropolymer coated silicon.

Keywords: contact angle, robust superhydrophobicity, slurry abrasion, black silicon, Teflon, hot embossing

1. Introduction

Superhydrophobic, water repellent surfaces are under intense study. Inspired by the Lotus-effect [1][2], many groups have sought inspiration from nature. Applications of superhydrophobic surfaces include droplet based microfluidics [3][4][5] and self cleaning [1]. The key defining property of superhydrophobic surfaces is very low adhesion of water droplets leading to droplets easily rolling off the surface. Superhydrophobic surfaces combine a low surface energy (high contact angle) surface chemistry to properly designed roughness parameters, which lead to droplets being in the so called Cassie state [6] so that they sit partly on air and only partly on solid surface. This air/solid composite state enhances the natural hydrophobicity of the surface and leads to low contact angle hysteresis and droplets easily rolling off the surfaces [7][8]. The stability of the Cassie state is a key requirement for superhydrophobic surfaces [9], since other possible wetting states (e.g. Wenzel or mixed states [7]) have much higher adhesion and thus do not lead to low angle roll-off. In addition to these requirements, the apparent contact angles [10] of superhydrophobic surfaces should be high.

Dual scale roughness is highly beneficial for superhydrophobicity. The main effect of dual scale roughness is to stabilize the Cassie state [8]. Many additive, subtractive and replication based fabrication methods have been used to achieve multiple roughness scales [11][12][13][14][15][16]. Template-based deposition, natural objects as molds, etching (wet, dry, electrochemical), electrodeposition, CVD, electrospinning and other fiber-based approaches, scratching and stretching, spray deposition, phase separation, colloidal assembly, sol-gel methods and various combinations have been successfully employed.

The combinations of superhydrophobic and abrasion resistant surfaces remain rare [17]. Various composite structures have been made that exhibit durable superhydrophobicity, for example polymer-coated roughened alumina where the extra volume created by the roughening process acts as a reservoir for polymer which can recover after damaging [18] or fluoroalkyl-coated silica nanoparticles in PDMS [19]. In [20], clay and polymer are combined to create easily applicable superhydrophobic coating while Zhu et al. [21] present a composite metal fluoropolymer surface. Recently, Jin et al. [22] demonstrated a superomniphobic aerogel surface which retained its properties after sandpaper scratching. An alternative approach is found in self-healing materials, where for example diffusion of oligomers to surface restores the superhydrophobicity [23].

From the viewpoint of durability under harsh conditions, coatings and inherently hydrophobic materials are very different. Most coatings used to create superhydrophobic surfaces are very thin, ranging from monomolecular layers to a few hundreds of nanometers. A common approach is to use perfluorinated films, either by evaporation, spin coating, spraying, or by plasma deposition [24]. In [15], silicone nanofilaments were synthesized on silicon micropillars to form a dual scale structure.

Teflon™ (PTFE) and Teflon-like perfluoro compounds are difficult to micromachine. Etching of PFTE is one way to create the required dual scale roughness [25]. Etching, however, requires lithography and suitable etch mask which makes it time consuming. Etch rates of polymers are very slow and only fairly

shallow structures can be made. Superhydrophobic surfaces out of Teflon have also been made by scraping [26] and through the use of sacrificial colloids [27].

Wear testing of superhydrophobic surfaces is usually approached from two directions: from hard materials direction with Taber, pin-on-disc and abrasion tests [28] as well as indentation and scratching [29], or from textile industry direction with washing [19] and wiping tests [30]. Micro and nanostructure wear resistance is topic that is poorly known. Some work has been carried out on sliding wear for rotary MEMS [31] but for most applications there is scarce information available.

In this paper we present a slurry abrasion test which is a wear test for superhydrophobicity that takes place under water. We also introduce perfluoropolymer CYTOP™ micromachining to take benefit of Teflon-like bulk properties in creating superhydrophobic surfaces. The samples in this paper are fabricated by hot embossing CYTOP™ with a PDMS elastomer stamp. We show how the resulting micro and nanostructured surfaces retain their superhydrophobicity under abrasion, and compare these inherently hydrophobic perfluoropolymer structures to identical silicon micro and nanostructures which are coated by a thin fluoropolymer film.

2. Experimental

2.1 Silicon Masters

CYTOP micropillars, nanopillars and dual scale micro-nanopillars were fabricated by hot embossing (Fig.1). First, masters were created from silicon using cryogenic deep reactive ion etching (DRIE) (Plasmalab System 100, Oxford Instruments, Bristol, UK). Silicon micropillars were fabricated using AZ-5214 photoresist as the masking material. Silicon nanopillars were fabricated through a maskless "black silicon" process [32]. Two types of combined dual scale micro-nanopillars were fabricated. First version had nanopillars both at the top and the bottom plane of the micropillars. These were fabricated by fabricating the micropillars, removing the photoresist and then etching the whole substrate using the black silicon process. The second version had nanopillars only on top of the micropillars. These were fabricated by etching the whole wafer with the black silicon process and then doing the lithography and micropillar etching, with a final isotropic etching step for removing the nanopillars from the bottom plane. Working stamps for hot embossing were fabricated from the masters using h-PDMS/PDMS casting, as explained in a previous publication [33]. We have noticed that utilizing a hard PDMS layer improves the fidelity of replicating nanostructures into polymers by hot embossing.

2.2 CYTOP Processing

CYTOP (CTL-809M from Asahi Glass) was spin coated (600rpm, 40s) on top of silicon wafers and baked for 30 min at 50°C followed by 90 min at 180°C. The resulting layer thickness was around 7 μm. The hot embossing was done using AWB-04 wafer bonder (Applied Microengineering Ltd., Didcot, UK). The stamp and the substrate were first both heated to 148°C and then brought into contact in a vacuum. The embossing force was 5kN and the duration was 15 min. The system was then cooled down, after

which the substrate and the stamp were separated by manual peeling. CYTOP etching for residual layer removal was done using RIE (Plasmalab 80+, Oxford Instruments, Bristol, UK) oxygen plasma. The parameters were RF power 200 W, pressure 250 mTorr, 45 sccm O_2 and 5 sccm Ar. The etch rate of CYTOP with this recipe was 400 nm / minute.

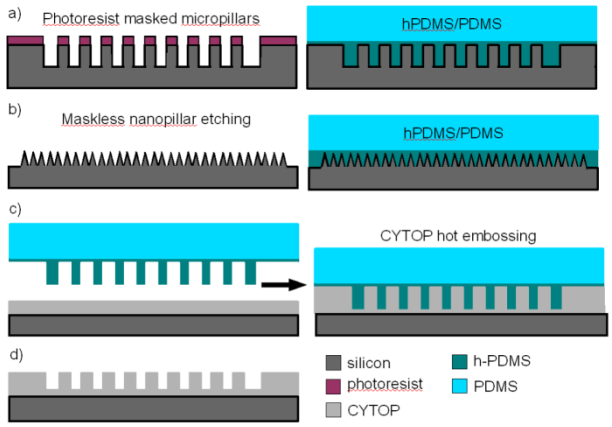

Figure 1. *Fabrication Scheme for CYTOP pillars. a), b) Micropillar, nanopillar and micro-nanopillar silicon masters are fabricated through plasma etching and a working stamp is made out of hPDMS/PDMS by spin coating and casting. c) CYTOP is spin coated and cured on a silicon wafer, and the layer is hot embossed using the working stamp. d) Final CYTOP structures after stamp release. Note that the residual layer guarantees that the surface is totally covered with CYTOP unless it is specifically removed.*

2.3 Abrasive Slurry Testing

Our rotary slurry test set-up is shown in Figure 2. The set-up comprises of a modified biostat device (Biostat M from B. Braun) with a custom sample holder (Fig. 2). The sample holder is connected directly to the motor by a long steel rod. The sample holder was designed to simultaneously hold four 10 mm x 10 mm test pieces. The surface of the sample was tilted so that the angle of impact was 73°. The distance of the sample from the rotation was 25 mm as measured from the centre of the sample. With the device, we can control both the temperature and the rotation rate. For these experiments, the temperature was fixed at room temperature and the rotation was set at 900 rpm for the main abrasion experiment. The slurry we used for the main abrasion experiment consisted of 10 % (by weight) solution of 30 μm alumina particles in water. The slurry was contained in a 500 ml glass beaker equipped with four stator plates to prevent flow of the slurry. Two parallel runs were performed for each of the samples.

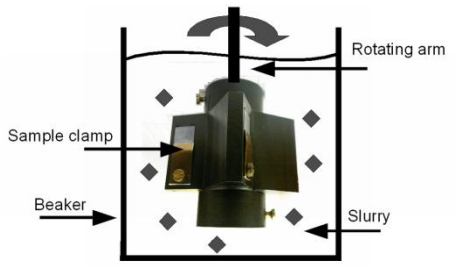

Figure 2. Rotary abrasive slurry test setup.

2.4 Contact Angles and Sliding Angles

The apparent contact angles were measured by the sessile droplet method (CAM 101, Biolin Scientific, Espoo, Finland). The contact angles on each chip were measured from five predetermined spots (the same spots on all samples) and averaged. The sliding angles were measured on an in house built device using 10 μl droplets of deionized water.

2.5 Scanning Electron Microscopy

Scanning electron microscopy (SEM) was performed utilizing Supra 40 (Carl Zeiss SMT, Oberkochen, Germany).

3. Results and Discussion

3.1 Micro and Nanopillars

Hot embossed single scale CYTOP micro and nanopillars are shown in Figure 3. The replication of silicon structures into CYTOP via hot embossing with a hPDMS/PDMS composite is accurate, like was previously reported for PMMA [32]. The micropillar geometry consisted of 10 μm diameter cylinders in a 20 μm pitch rectangular lattice, and the height of the pillars was between 10 μm - 12 μm. The nanopillars were cone shaped, roughly 3 μm in height and 500 nm in base diameter. The apparent contact angles of the unabraded CYTOP micro and nanopillars were 156° and 167°, respectively. Droplets also easily roll off the samples without leaving a trace of water behind at low tilting angles (13° and 10° respectively), showing that the droplets are in a Cassie state and that the surface has low contact angle hysteresis.

Several points of the embossing process are noteworthy. First, the same hot embossing recipe was used for both micro and nanopillars as well as dual scale pillars. Second, we were able to replicate silicon micropillars up to 12 μm in height (higher structures were not attempted) even though the initial spin coated CYTOP layer was only around 6 μm in thickness. This was possible since the actual micropillars only covered around 20% of the projected surface area. Third, the thickness of the residual layer for the micropillar structure was around 900 nm (Fig. 3b), while for the nanopillars it was around 3 μm (Fig. 3e). The residual layer ensures that the embossing process produces a surface with uniform hydrophobic

surface chemistry with a single step, which is beneficial for anti-adhesive applications. However, some applications might prefer surfaces where the superhydrophobic micropillars are on top of a more chemically reactive substrate, such as glass or metals. We were able to fabricate such surfaces by etching away the residual layer away in oxygen plasma, thus revealing the underlying substrate (Fig. 3c). These types of functional surfaces are not that simple to fabricate in general, since most of the time a coating is used and the coating typically also covers the substrate.

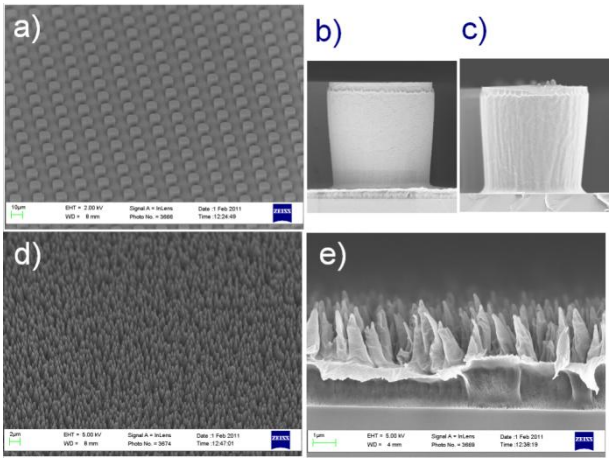

Figure 3. CYTOP micro and nanopillars. a) CYTOP micropillars, 10 μm diameter, 10 μm height, 20 μm pitch b) CYTOP micropillar before residual layer removal c) CYTOP micropillar after residual layer removal d) CYTOP nanopillars e) Sideview of CYTOP nanopillars

3.2 Dual Scale Pillars

Two types of dual scale pillars were fabricated. Fig. 4a (silicon master) and Fig. 4b (CYTOP) show a dual scale structure which has nanopillars both at the top of the micropillars and also covering the base substrate level, while the structure shown in Fig. 4c (silicon master) and Fig. 4d (CYTOP) has nanopillars only on top of the micropillars. The apparent contact angles of both dual scale pillars were very high (≈ 170°) and the sliding angles were very low.

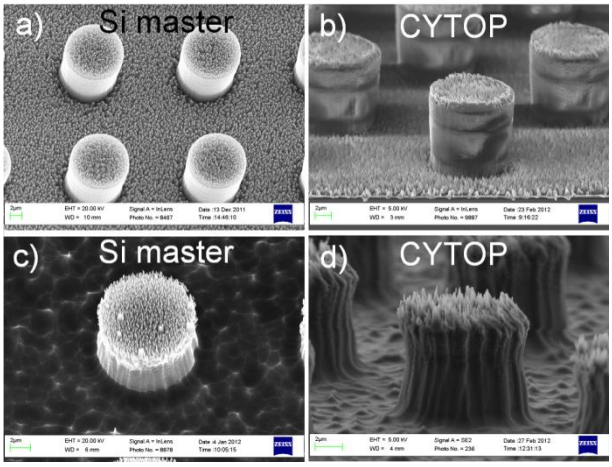

Figure 4. Dual scale CYTOP pillars. a) silicon micropillar master with nanopillars on the top and at the bottom. b) CYTOP micropillars with nanopillars on the top and at the bottom. c) Silicon micropillar master with nanopillars on the top. d) CYTOP micropillars with nanopillars on the top

3.3 Abrasive Slurry Test

We developed an abrasive slurry setup for testing the abrasion resistance of superhydrophobicity. The sample to be tested is rotated in slurry and the erosion results from direct impacts between the particles and the surface of the sample. The beaker holding the slurry contains stators to prevent the slurry from picking up momentum. Our setup is designed to be a much milder form of the slurry test that is suitable for soft matter, micro and nanostructures and thin-film coatings. The extent of erosion in a slurry test depends on the composition, size, and shape of the eroding particles, their velocity and angle of impact, and the composition and microstructure of the surface being eroded [28]. The angle of impact was fixed to be 73° but for the other parameters, a preliminary study was performed in order to determine satisfactory parameters for superhydrophobicity testing. In this test, we used fluoropolymer coated planar silicon and fluoropolymer coated silicon micropillars as the samples (same samples as the reference samples used for the main abrasion experiment). With 2 % solution of 6 μm alumina particles, we saw very little abrasion even after 4 hours of 900 rpm abrasion. With 1 % solution of 30 μm alumina particles we started to see some erosion at 900 rpm but not 500 rpm or 700 rpm. Finally, we settled with a 10 % solution of 30 μm alumina particles and fixed the rotation rate at 900 rpm. With these parameters, we saw noticeable erosion in the timescale of hours.

3.4 Abrasion Resistance of Superhydrophobicity

Tables 1 and 2 present the results of the abrasion tests for CYTOP and silicon micro and nanopillars. The silicon pillars had identical geometries to the CYTOP pillars (they were made with the same process as the original masters for CYTOP embossing) and had a thin (≈ 40 nm thick) fluoropolymer coating for achieving superhydrophobicity. This fabrication scheme, masters compared to embossed structures, allowed us to independently assess the effect of the geometry and the composition of surfaces. The level of superhydrophobicity at various stages of abrasion was characterized by the sliding angle (Table 1) and the apparent contact angle (Table 2) of the surfaces.

The results show that for all surfaces, the sliding angle steadily increased and the apparent contact angle decreased with increased level of abrasion. The clearest qualitative difference observed was between the abrasion resistances of CYTOP structures as compared to the fluoropolymer coated silicon structures. In the case of the inherently hydrophobic CYTOP structures, the droplets stayed in a Cassie state even after the full 4 hours of abrasion and could roll off, albeit at steeper angles than before the abrasion. In comparison, the fluoropolymer coated silicon samples lost their roll-off property during the first 60 minutes of abrasion and became sticky to the extent that even a tilt of 90° or 180° could not get the droplets to roll or fall off the surfaces.

The reason for this difference lies in the chemical composition of the surfaces. The CYTOP micro and nanopillars are inherently hydrophobic, which is highly beneficial for durability of the superhydrophobicity under wear [17]. Even if the structures themselves are mechanically damaged, there will not be a change in the surface chemistry, which means that the barrier between the Cassie state and other wetting states can be maintained. However, in the case of silicon, at the point when the coating layer has been abraded away, the surface chemistry changes to that of underlying silicon, which is slightly hydrophilic. In the absence of either overhanging [34] or air-trapping [16] geometries, the chemistry change into hydrophilic removes the transition barrier, which causes the droplets to fall into either a full Wenzel state or alternatively a mixed state in case the change in surface chemistry is only partial. The change in the wetting state explains why the droplets can no longer roll off the surfaces, even though in many cases relatively high apparent contact angles were still measured for the silicon samples.

The effect of the abrasion on the surface chemistry was also revealed in the apparent contact angle measurements of planar reference layers of CYTOP and fluoropolymer coated silicon. The planar CYTOP layer remained practically unchanged throughout the four hour abrasion experiment (from 108° to 106°), while the fluoropolymer coated silicon surface gradually lost its hydrophobicity and became hydrophilic as the coating eroded (from 95° to 64°).

Figure 5 shows SEM micrographs of all four surfaces after 4 hours of abrasion. The results clearly indicate that the topography of the micropillar surfaces remained largely intact while the topographies of the nanopillar surfaces show severe erosion. However, in spite of the severe erosion, droplets on the CYTOP nanopillar surfaces were able to roll off even after 4 hours of abrasion, although the roll off angle steadily increased from 10° to 32°. This increase in the sliding angle was much larger than the corresponding increase on the CYTOP micropillars (from 13° to 21°), demonstrating that the abrasion resistance of the topography is also important even if it is of secondary importance to the preservation of the surface chemistry.

Table 1. Sliding angles of CYTOP and silicon micro and nanopillars.

	Untreated	**60 min**	**120 min**	**240 min**
CYTOP Micropillars	13°	21°	21°	21°
CYTOP Nanopillars	10°	18°	22°	32°
Silicon Micropillars	30°	>90° (STICKY)	>90° (STICKY)	>90° (STICKY)
Silicon Nanopillars	11°	>90° (STICKY)	>90° (STICKY)	>90° (STICKY)

Table 2. Apparent contact angles of CYTOP and silicon micro and nanopillars.

	Untreated	**60min**	**120min**	**240min**
CYTOP Micropillars	156°	112°	111°	110°

CYTOP Nanopillars	167°	144°	140°	132°
Silicon Micropillar	155°	131°	124°	108°
Silicon Nanopillars	165°	141°	136°	125°
Planar CYTOP	108°	107°	107°	106°
Planar Coated Silicon	95°	92°	74°	64°

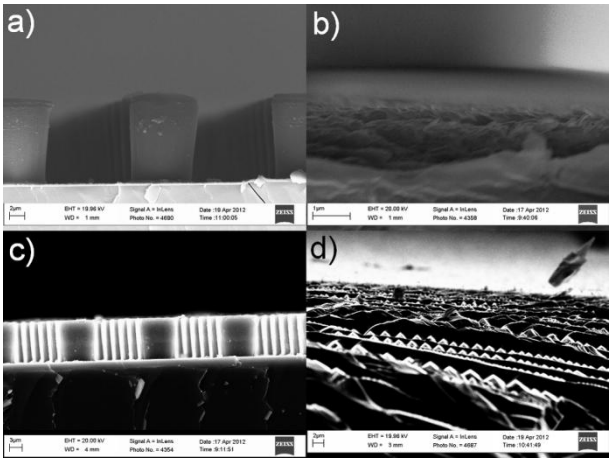

Figure 5. CYTOP and silicon micro and nanopillars after 4 hours of abrasion. a) CYTOP micropillars b) CYTOP nanopillars c) silicon micropillars d) silicon nanopillars.

4. Conclusions

The topic of durable superhydrophobicity is important for bringing the recent theoretical and experimental advances into practical applications (e.g. solar panels, touch screen devices). Abrasion testing of superhydrophobic micro and nanostructures is in its infancy, and novel ways to quantify abrasion resistance are much in need. We presented a slurry abrasive testing setup, and utilized it for studying silicon and CYTOP micro and nanopillars. The results showed that the first priority for achieving abrasion resistant superhydrophobicity should be retaining hydrophobic surface chemistry under wears, while retaining the physical topography should be the second priority. It is interesting to note that many of the geometries that have been proposed to provide maximum stability of the Cassie state, including e.g. slender pillars with high aspect ratios or nanoscale pillars on top of microstructures [8], are quite vulnerable to mechanical abrasion. One future avenue for research is optimization of geometries simultaneously for both abrasion resistance and the stability of the Cassie state.

Acknowledgements

P. S. received funding from Graduate School of Chemical Sensors and Microanalytical Systems (CHEMSEM). Part of the research was performed at the Micronova Nanofabrication Centre of Aalto University.

References

[1] W. Barthlott, C. Neinhuis, Purity of the sacred lotus, or escape from contamination in biological surfaces, Planta. 202 (1997) 1–8.
[2] A. Marmur, The Lotus Effect: Superhydrophobicity and Metastability, Langmuir. 20 (2004) 3517–3519.
[3] V. Jokinen, R. Kostiainen, T. Sikanen, Multiphase Designer Droplets for Liquid-Liquid Extraction, Advanced Materials. (2012).
[4] E. Ueda, P.A. Levkin, Emerging Applications of Superhydrophilic-Superhydrophobic Micropatterns, Advanced Materials. 25 (2013) 1234–1247.
[5] H. Mertaniemi, V. Jokinen, L. Sainiemi, S. Franssila, A. Marmur, O. Ikkala, et al., Superhydrophobic Tracks for Low-Friction, Guided Transport of Water Droplets, Adv. Mater. 23 (2011) 2911–2914.
[6] A.B.D. Cassie, S. Baxter, Wettability of porous surfaces, Transactions of the Faraday Society. 40 (1944) 546–551.
[7] E. Bormashenko, Wetting transitions on biomimetic surfaces, Philosophical Transactions of the Royal Society A: Mathematical, Physical and Engineering Sciences. 368 (2010) 4695–4711.
[8] N.A. Patankar, Mimicking the Lotus Effect: Influence of Double Roughness Structures and Slender Pillars, Langmuir. 20 (2004) 8209–8213.
[9] L. Barbieri, E. Wagner, P. Hoffmann, Water wetting transition parameters of perfluorinated substrates with periodically distributed flat-top microscale obstacles, Langmuir. 23 (2007) 1723–1734.
[10] A. Marmur, Soft contact: measurement and interpretation of contact angles, Soft Matter. 2 (2006) 12.
[11] Y.Y. Yan, N. Gao, W. Barthlott, Mimicking natural superhydrophobic surfaces and grasping the wetting process: A review on recent progress in preparing superhydrophobic surfaces, Advances in Colloid and Interface Science. 169 (2011) 80–105.
[12] T. Rasilainen, M. Suvanto, T.A. Pakkanen, Anisotropically microstructured and micro/nanostructured polypropylene surfaces, Surface Science. 603 (2009) 2240–2247.
[13] G. Jin, G. Kim, Pressure/Electric-Field-Assisted Micro/Nanocasting Method for Replicating a Lotus Leaf, Langmuir. 27 (2011) 828–834.
[14] H. Teisala, M. Tuominen, M. Aromaa, M. Stepien, J.M. Mäkelä, J.J. Saarinen, et al., Nanostructures Increase Water Droplet Adhesion on Hierarchically Rough Superhydrophobic Surfaces, Langmuir. 28 (2012) 3138–3145.
[15] T. Verho, J.T. Korhonen, L. Sainiemi, V. Jokinen, C. Bower, K. Franze, et al., Reversible switching between superhydrophobic states on a hierarchically structured surface, PNAS. (2012).
[16] E. Bormashenko, T. Stein, G. Whyman, Y. Bormashenko, R. Pogreb, Wetting Properties of the Multiscaled Nanostructured Polymer and Metallic Superhydrophobic Surfaces, Langmuir. 22 (2006) 9982–9985.

[17] T. Verho, C. Bower, P. Andrew, S. Franssila, O. Ikkala, R.H.A. Ras, Mechanically Durable Superhydrophobic Surfaces, Advanced Materials. 23 (2011) 673–678.
[18] S. Höhne, C. Blank, A. Mensch, M. Thieme, R. Frenzel, H. Worch, et al., Superhydrophobic Alumina Surfaces Based on Polymer-Stabilized Oxide Layers, Macromolecular Chemistry and Physics. 210 (2009) 1263–1271.
[19] H. Zhou, H. Wang, H. Niu, A. Gestos, X. Wang, T. Lin, Fluoroalkyl Silane Modified Silicone Rubber/Nanoparticle Composite: A Super Durable, Robust Superhydrophobic Fabric Coating, Advanced Materials. 24 (2012) 2409–2412.
[20] I.S. Bayer, A. Brown, A. Steele, E. Loth, Transforming Anaerobic Adhesives into Highly Durable and Abrasion Resistant Superhydrophobic Organoclay Nanocomposite Films: A New Hybrid Spray Adhesive for Tough Superhydrophobicity, Applied Physics Express. 2 (2009) 125003.
[21] X. Zhu, Z. Zhang, X. Men, J. Yang, K. Wang, X. Xu, et al., Robust superhydrophobic surfaces with mechanical durability and easy repairability, Journal of Materials Chemistry. 21 (2011) 15793.
[22] H. Jin, X. Tian, O. Ikkala, R.H.A. Ras, Preservation of Superhydrophobic and Superoleophobic Properties upon Wear Damage, ACS Applied Materials & Interfaces. 5 (2013) 485–488.
[23] Y. Li, L. Li, J. Sun, Bioinspired Self-Healing Superhydrophobic Coatings, Angewandte Chemie International Edition. 49 (2010) 6129–6133.
[24] V. Jokinen, L. Sainiemi, S. Franssila, Complex Droplets on Chemically Modified Silicon Nanograss, Adv. Mater. 20 (2008) 3453–3456.
[25] T. Kobayashi, K. Shimizu, S. Konishi, Investigation of Denaturation of Hydrophobic Perfluoropolymer Surfaces and Their Applications for Micropatterns on Biochip, Journal of Microelectromechanical Systems. 21 (2012) 62–67.
[26] C. Guo, S. Wang, H. Liu, L. Feng, Y. Song, L. Jiang, Wettability Alteration of Polymer Surfaces Produced by Scraping, Journal of Adhesion Science and Technology. 22 (2008) 395–402.
[27] P. van der Wal, U. Steiner, Super-hydrophobic surfaces made from Teflon, Soft Matter. 3 (2007) 426.
[28] D.M. Kennedy, M.S.J. Hashmi, Methods of wear testing for advanced surface coatings and bulk materials, Journal of Materials Processing Technology. 77 (1998) 246–253.
[29] A. Skarmoutsou, C.A. Charitidis, A.K. Gnanappa, A. Tserepi, E. Gogolides, Nanomechanical and nanotribological properties of plasma nanotextured superhydrophilic and superhydrophobic polymeric surfaces, Nanotechnology. 23 (2012) 505711.
[30] C. Su, Y. Xu, F. Gong, F. Wang, C. Li, The abrasion resistance of a superhydrophobic surface comprised of polyurethane elastomer, Soft Matter. 6 (2010) 6068.
[31] I.S.Y. Ku, T. Reddyhoff, A.S. Holmes, H.A. Spikes, Wear of silicon surfaces in MEMS, Wear. 271 (2011) 1050–1058.
[32] L. Sainiemi, V. Jokinen, A. Shah, M. Shpak, S. Aura, P. Suvanto, et al., Non-Reflecting Silicon and Polymer Surfaces by Plasma Etching and Replication, Adv. Mater. 23 (2011) 122–126.
[33] S. Aura, V. Jokinen, L. Sainiemi, M. Baumann, S. Franssila, UV-Embossed Inorganic-Organic Hybrid Nanopillars for Bioapplications, Journal of Nanoscience and Nanotechnology. 9 (2009) 6710–6715.
[34] A. Tuteja, W. Choi, M. Ma, J.M. Mabry, S.A. Mazzella, G.C. Rutledge, et al., Designing Superoleophobic Surfaces, Science. 318 (2007) 1618–1622.